INTUITIVE

INnovative Network for **T**raining in To**U**ch **I**nterac**TIVE** Interfaces

Grant agreement: #861166 H2020-MSCA-ITN-2019

Start date: 2019-10-01 End date: 2023-09-30

Deliverable reporting document

Deliverable no: 4.4		WP: 4
Deliverable name: Sensors with memory	Type: Demonstrator	Dissemination level: Public
Due Delivery date: 31 March 2022		Date delivered: 1 April 2022

Description:

Demonstrator of the properties of the sensors based on memristive device

Highly sensitive and biodegradable pressure sensor with sandwiched memristor structure

Note: Journal article has been submitted.

Abstract:

Highly sensitive pressure sensor with features such as biocompatibility, biodegradability, and flexibility are needed in applications such as robotics, prosthesis, medical implants, and wearable electronics. However, due to material limitations or technological bottlenecks it is challenging to fabricate a pressure sensor with all these attributes at the same time. Herein, we present a silk-Polyvinyl Alcohol (S-PVA) composite nanofiber-based flexible, biocompatible, and biodegradable capacitive pressure sensor developed using a facile and cost-effective screen-printing approach. The screen-printed silver was used as the top and bottom electrode with flexible and biodegradable chitosan as a substrate. The device exhibited extremely wide pressure sensing range varying from ~1 kPa to 800 kPa with a maximum sensitivity of ~2.83 kPa^{-1} (<10kPa) and fast response and recovery time of ~35 and ~40 ms. The high sensitivity in the low-pressure region is primarily due to the high porosity and surface area, and reduction in the effective distance between the multilayers of 1D S-PVA nanofibers. The device shows excellent cyclic repeatability and good stepwise cyclic increment in both low- and high-pressure regions for more than $2x10^3$ and $3.2x10^3$ cycles respectively. Finally, the biodegradability tests reveal that the device completely dissolved in pure DI water at room temperature in less than 24 hours. Thus, the novel S-PVA composite based nanofiber serves as an excellent biomaterial and paves the path for next generation wearable and implantable medical device applications.

I. Introduction

High performance pressure sensors are needed in numerous applications such as biomedical devices, robotics, and interactive systems etc. For example, as part of electronic skin (e-skin), the pressure sensors provide a measure of contact force, which is needed for haptic feedback-based action in robotics, prosthesis, and rehabilitation devices such as smart gloves[1,2]. Likewise, they are

used in different types of wearable systems to monitor physiological parameters such as blood pressure or the pressure applied with compression bandage at a wound site or in implantable systems for cardiovascular or blood flow monitoring.[3-10] As a result, various types of pressure sensors based on different transduction mechanisms (e.g. piezoresistive[11-15], piezoelectric[16], capacitive[17-19], etc.), have been explored to meet varying performance requirements (e.g., sensitivity, resolution, detection range etc.) of these applications. Recently, the application requirements have also led to a shift in the research towards obtaining devices with features such as flexibility and conformability etc[20-22], which are needed to ensure reliable contact between the sensor and the curvy surfaces such as the human skin.[23] Whilst these are interesting advances, various health monitoring and implantable systems also require pressure sensors to be made of biocompatible, and biodegradable materials.[24-26,10] However, most of the high-performance pressure sensors reported so are not biocompatible and biodegradable. In this regard, the single use sensors made from biodegradable materials could offer interesting solutions as besides ensuring the hygiene requirements they will also be free from other issues related to wearable systems such as washability. Furthermore, degradable sensors could also help address the rapidly growing challenges related to medical and electronic waste. [27] Considering this background, herein we present silk - Polyvinyl Alcohol (PVA) nanofibers based biodegradable wide-range pressure sensors on chitosan/ Polyvinyl chloride (PVC) substrate.

The fabrication of pressure sensor which simultaneously exhibits high performance and biodegradability is quite challenging. A careful selection of materials and fabrication method is important for the development of degradable pressure sensors as many of the above applications require extreme sensitivity over a wide pressure range, which is still lacking in most of the current state-of-the-art pressure sensors. For example, highly sensitive sensors are needed to detect the weak bio-signals which typically fall in the low-pressure region (<50kPa)[28] as well as to measure the mid-to high pressure signals in prosthesis/robotics for stable grasping or walking. The trade-off between the sensitivity and pressure detection range makes it challenging to attain both at the same time. To address this issue, sensors with microstructures such as microspheres, pyramids, microgrooves, and micro and nanopillars, etc. on elastomeric materials have been developed using complex methodologies.[19,29-31] These techniques have led to high sensitivity in limited pressure regions and there is still a need for sensitive sensors capable of operating over wide pressure ranges. A potential solution is to use polymeric nanofibers prepared using a simple, cost-effective,

and solution processing-based electrospinning approach.[32] The nanofibers provide numerous advantages, such as lightweight, low-cost, ease of preparation, excellent dielectric strength, higher porosity, and superior mechanical flexibility. In addition, electrospinning is compatible with the widely used biocompatible and biodegradable polymers such as silk, cellulose, chitosan, PVA, PVP etc. [33,34] For these reasons, electrospinning has been used here to develop the silk-PVA (S-PVA) nanofibers based biodegradable pressure sensor. The Food and Drug Administration (FDA)-approved silk also stands out among various natural biodegradable materials (e.g., collagen, cellulose, chitosan, silk fibroin, egg albumin etc. [35, 38-41]), owing to its natural abundance, low-cost, outstanding mechanical flexibility, superior biocompatibility, and the possibility to obtain programmable or controlled degradation. Furthermore, the silk fibroin offers excellent properties such as optical transparency, piezoelectricity, high dielectric strength, solution processability, and structural tunability.[42] For these reasons, the S-PVA nanofibers have been used here to develop the low-cost, flexible, biodegradable capacitive pressure sensor on chitosan/PVC substrate. The S-PVA nanofibers in the presented sensor are sandwiched between screen printed silver electrodes. The S-PVA based pressure sensor can operate in a wide pressure range (1kPa to 800kPa) and exhibits the maximum sensitivity of 2.83 kPa^{-1} in the low-pressure region (<kPa). The fabricated device exhibits fast response and recovery times of 30 and 40 ms respectively and an excellent stability (for more than 2500 cycles). The biodegradability tests performed on the as fabricated pressure sensors show complete dissolution in DI water (at room temperature) in less than 24 hours.

II. Results and discussions

Silk fibroin is one of the best materials for biodegradable and biocompatible devices as discussed earlier. Moreover, the dielectric strength of the silk fibroin is high, which makes it an ideal candidate for the capacitive pressure sensors. Figure 1 shows the schematic illustration of the step-by-step process for the preparation of pure silk fibroin solution, electrospinning, and the device structure. From previous studies, we know that the addition of PVA enhances the mechanical flexibility and thermal stability.[43] The solution viscosity and flow rate play an important role in the formation of uniform and long nanofibers with thinner diameters. A lower concentration of 8 wt.% of silk solution resulted in the formation of the nanofibers with many beads. On other hand, the higher concertation of 13 wt.% was highly viscous and not suitable for electrospinning. The

optimized and moderate concentration of 10 wt.% was finally chosen for the electrospinning of both silk and S-PVA, as smooth and uniform nanofibers are formed at this concentration.

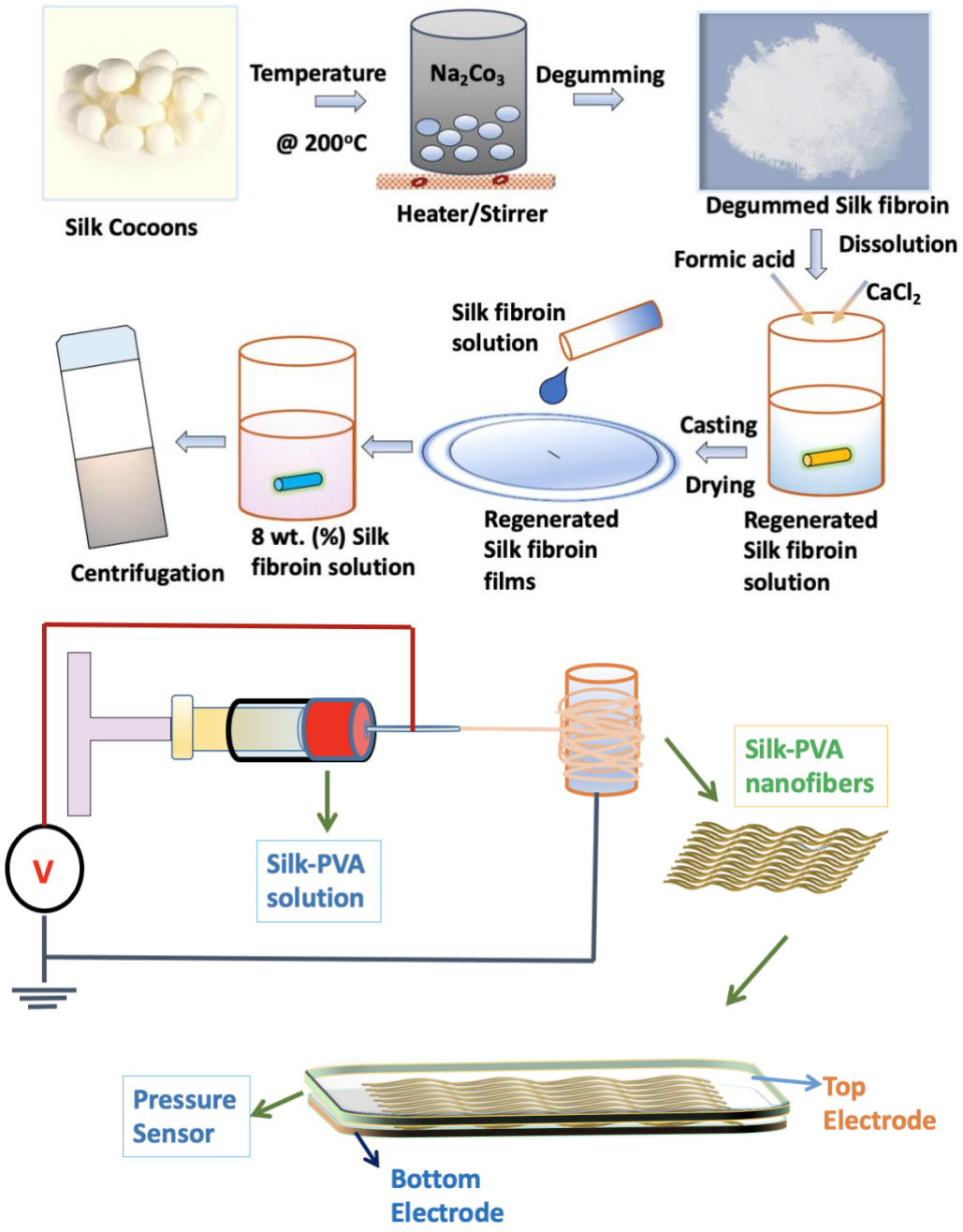

Figure1. Schematic showing complete process flow for the preparation of silk fibroin solution and detailed step by step process followed for preparation of nanofibers and fabrication of device structure with patterned gold/silver on PVC/chitosan as top and bottom electrode.

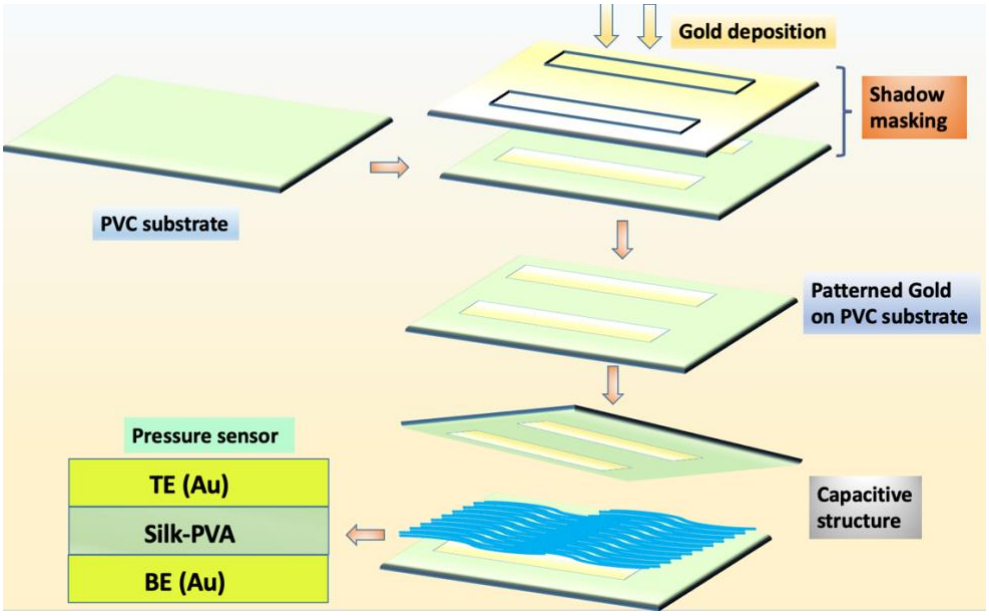

Figure 2. A detailed schematic showing complete fabrication process flow for the fabrication of the flexible capacitive pressure sensor using gold coated on PVC substrate as a top and bottom electrode with Silk-PVA nanofiber as a dielectric layer.

The optical image of the electro spun S-PVA nanofiber (after peeling off few layers) is shown in figure 3a showing very light weight and greater mechanical flexibility. Figure 3b shows the XRD spectrum of S-PVA nanofibers with a diffraction peak at 2θ angles of 20.27° and 24.9°, which correspond to Silk-II and Silk-I structure respectively.[44] These results reveal that the S-PVA composite nanofibers exhibit mixed structures with dominant amorphous (α helices) nature than crystalline domains (β sheets). To better understand the structural information, FTIR analysis was also carried out on the prepared 1D S-PVA nanofibers, which is shown in figure 3c. The peaks at wavenumbers 1227, 1509, and 1620 cm^{-1} confirm the presence of both alpha helices and beta sheets respectively, which is consistent with the literature.[45] The Fourier Self Deconvolution (FSD) analysis was performed to calculate the percentage of secondary structures which shows that the composite has 32% of alpha helices with 68% of other secondary structures. The obtained results suggest that the nanofibers are amorphous with higher alpha helices and exhibit enhanced mechanical flexibility as compared to the pristine silk nanofibers. Figure 3d shows the Raman spectra of S-PVA composite confirming the spectral peaks of both silk and PVA and matches well with the literature.[46] The spectral peaks at 1083cm^{-1}, 1226 cm^{-1}, and 1668 cm^{-1} confirm the presence of silk fibroin and the active bands at 885cm^{-1}, 1412 cm^{-1}, 1547cm^{-1} corresponds to PVA.

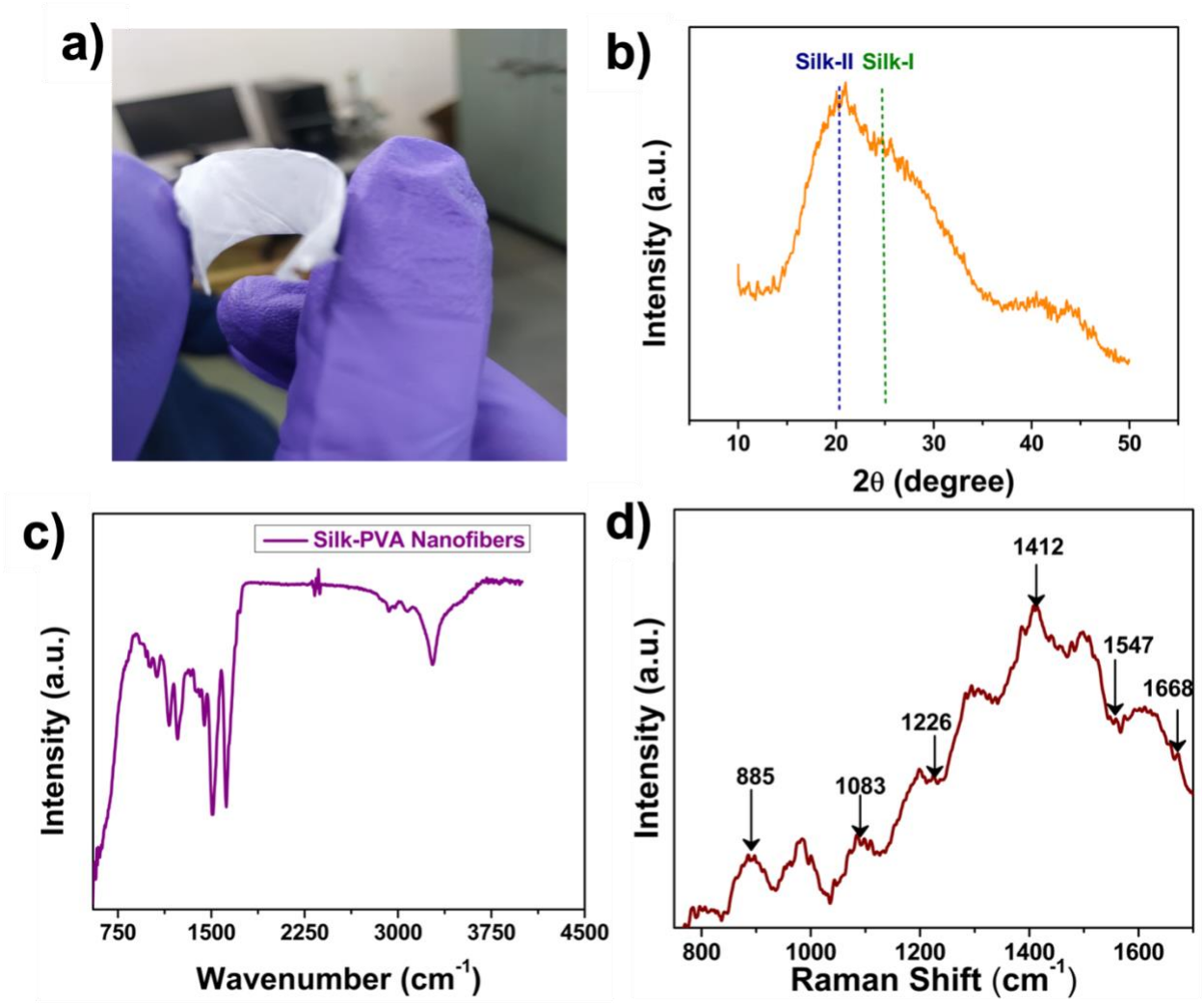

Figure 3. (a) Optical image of as prepared S-PVA peeled nanofiber film (b) XRD and (c) FTIR spectrum (d) RAMAN spectra of silk-PVA composite film for structural and chemical characterization studies.

FE-SEM studies were performed on both the electrospun pristine silk and S-PVA composite based nanofibers, as depicted in figure 4. Figure 4a and 4c shows the high magnification images and figure 4b and 4d shows the low magnification images of both silk and its composite. The as prepared S-PVA nanofibers are multi-layered stacked 1D nanofibers, are highly uniform, porous with large surface area, and mechanically flexible. The high porosity and multilayer stacking help to achieve high sensitivity pressure sensors. Moreover, due to excellent tensile strength of as prepared nanofibers, the sensor can withstand higher pressure sensing in contrast to traditional polymer based thin films. The average diameter (approximately 300 nm and 85nm) for both the S-PVA and pristine silk fibroin was calculated using image J software as shown in the inset of figure. 4b and 4d.

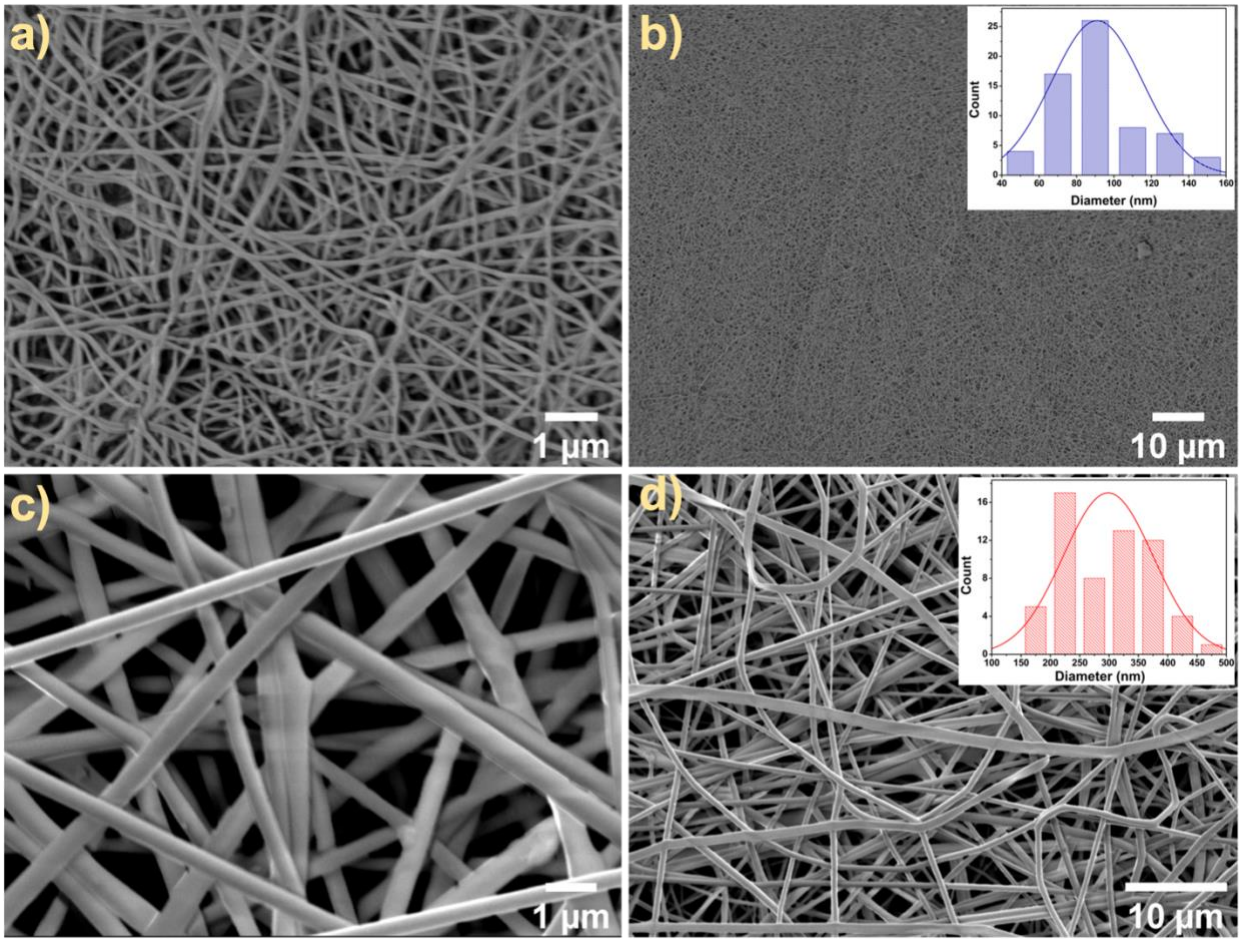

Figure 4. FESEM images (a) high and (b) low magnification images of pristine silk fibroin nanofibers (c) high and (d) low magnification images of silk-PVA composite based nanofibers with inset showing the average diameter of the nanofibers.

To achieve a thicker nanofiber film with stacked multilayers, the electrospinning was performed for longer durations of greater than 12 hours. The pressure sensor was fabricated using thin film of S-PVA nanofibers as the dielectric layer sandwiched between the patterned gold electrodes on the flexible PVC substrate. Furthermore, to demonstrate the fully biodegradable pressure sensor, the screen-printed silver on the flexible and biodegradable chitosan substrate was chosen as the electrodes. Thickness of the dielectric layer plays a crucial role in terms of achieving the desired sensitivity and the range of the pressure detection.[47] To achieve higher sensitivity, an optimized higher thickness of the nanofibers with large length, lower diameters and stacked layers were preferred, which is well known from the literature.[47] To this end, the chosen electrospinning time was greater than 12 hours. A very low flow rate 0.5mL/hr was used to achieve the highest film thickness of ~ 100µm. In principle, an ideal pressure sensor should be highly sensitive over a broad range of pressures and must have fast response and recovery time with stable cyclic repeatability.

Sensitivity (*S*) is one of the crucial parameters of a pressure sensor that determines the accuracy and effectiveness and is defined as the relative change in the capacitance ($\Delta C/C_0$) for the applied pressure (P) and is represented using the following equation 1[19]

$$S=\delta(\Delta C/C_0)/\ \delta(\Delta P) \ldots\ldots\ldots (1)$$

The sensitivity measurements were performed on the S-PVA based capacitive pressure sensor using an LCR meter connected to a PC having a custom-made LabVIEW software installed in it. To investigate the sensitivity, the response (relative change in capacitance) of the device under different applied pressures, a circular probe attached to a computer-controlled linear stage was used and pressure ranging from 1kPa to 800kPa was applied, as shown in figure 5a. For better understanding, the entire pressure range was divided into three different regions i.e., region (R_1) (1kPa<P<10kPa), region (R_2) (10kPa<P<200kPa), region (R_3) (200kPa<P<800kPa). In R_1, the device exhibits a linear change in capacitance for a linear increase in the applied pressure with a maximum sensitivity of ~2.83kPa^{-1}. Similarly, in the R_2, the device response was quite linear with a reduced change in the capacitance values and the calculated sensitivity value of ~0.63 kPa^{-1}. In R_3, the device response is linear but with a low capacitance variation in the high-pressure regime and reduced sensitivity of 2.3x10^{-4} kPa^{-1}. Importantly, the device is sensitive to a wide pressure range (1kPa to 800kPa), which is one of the highest among the current state-of-the-art capacitance-based pressure sensors as discussed in the table 1. The different sensitivities in the three regions might be due to the variation in the contact area at the interface of the top and bottom electrodes. The higher-pressure detection range might be due to the enhanced mechanical flexibility in the S-PVA composite due to the dominant amorphous structure which are alpha helices as confirmed by

the FSD analysis. The high sensitivity in the low-pressure region exhibited lower layer to layer distance and the higher contact area, resulting in the reduction of the overall effective distance.

Device-to-device variation is a significant parameter to determine the versatility of the fabrication methodology. To show the uniformity, three devices were fabricated under the same conditions. The variation in the mean and standard deviation in terms of sensitivity under three different pressure regions such as low, medium, and high were shown in figure 5b.

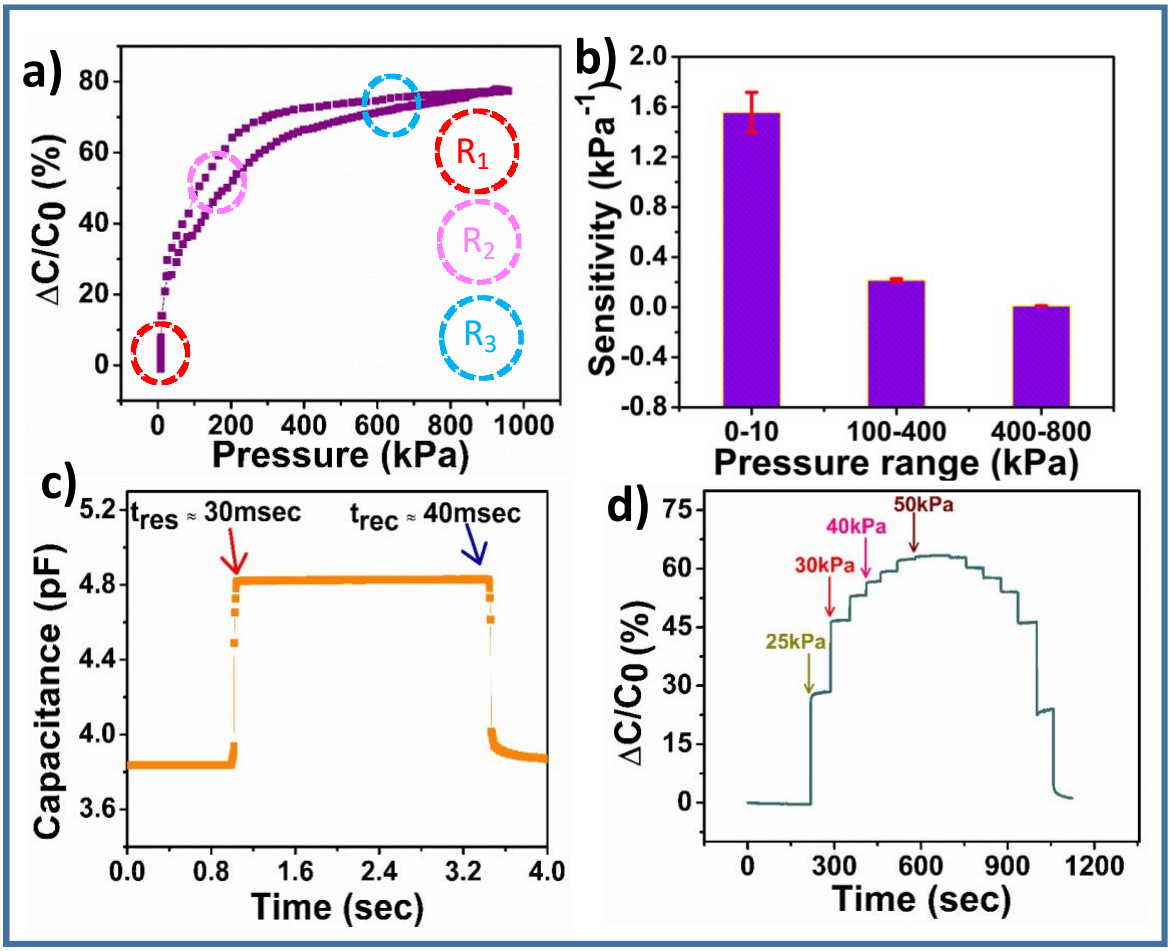

Figure 5. (a) Relative change in capacitance under different applied external pressures of the silk-PVA based pressure sensor (b) device to device variation in terms of calculated sensitivity for three devices under low, medium, and high-pressure regions (c) capacitance vs time plot showing both response time (t_{res}) 30 ms and recovery time (t_{rec}) of 40 ms (d) cyclic hysteresis plot with step wise increment under different pressure.

These results suggest that the variations in the high and medium pressure regions was negligible, whereas in the low-pressure region there is a minor deviation prominently due to the variation in the effective contact area between the electrodes resulting in the negligible variation in the capacitance values. The fast response and recovery times are also crucial for the real time applications. To understand how quickly the device responds, a plot showing the change in the capacitance with respect to time at low pressure of 20kPa was obtained, as shown in figure 5c. The response and recovery times were calculated from the time response plot by calculating the time interval between the 10% of initial value to the 90% of final value and 90% of final value to 10% of initial value respectively. The device shows a highly fast response and recovery times of 30 ms and 40 ms respectively, with the device instantly changing the capacitance from 3.8pF to 4.8pF. Further, the loading and unloading of different pressures ranging from 25-50kPa, with different step heights, was performed to demonstrate the device stability and reliability. Figure 5d shows the step response of the S-PVA-based pressure sensor showing excellent uniformity, stability, and reliability of performance with negligible variations.

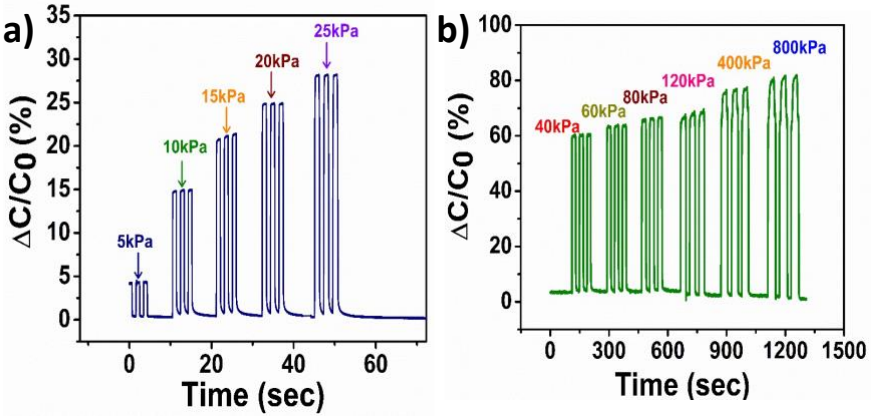

Figure 6. Cyclic response of the silk-PVA based capacitive pressure sensor under (a) low pressure regime, and (b) high pressure regime.

To further test the device reliability, stepwise cyclic tests were performed on the fabricated S-PVA device. Figure 6 shows the cyclic increment plot with a loading and unloading time of 3 sec, showing stable behaviour in from the low-pressure (Figure 6a) to ultra-high-pressure region (Figure 6b). The results reveal the unique wide pressure sensing capability of presented devices.

1D nanofibers are the one of the best candidates for capacitance-based pressure sensors due to their low cost, higher surface roughness due to porosity, and excellent mechanical robustness. The capacitance (C) is given by:

$$C=\varepsilon*(A/d) \ldots\ldots. (2)$$

where, C is the capacitance, A is the active area of the device, d is the distance between the top and bottom electrode, and ε is the permittivity of the dielectric material. Here, the active area of the device was kept constant and the variation in the capacitance was mainly due to the change in the distance between the electrodes and the dielectric constant of the S-PVA composite material.

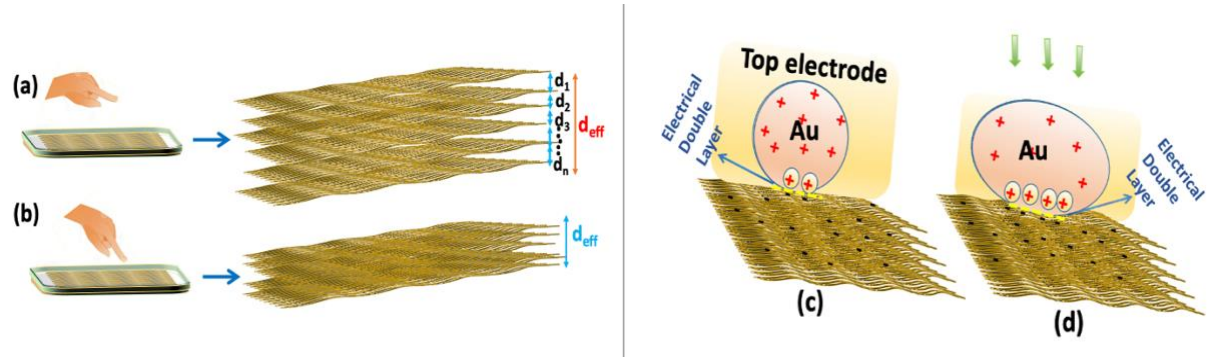

Figure 7. The sensing mechanism explaining the change in capacitance: (a) under no applied pressure condition, there is no change in the effective distance showing initial (lower) capacitance and (b) with applied pressure the effective distance decreases and hence the capacitance increases (c) lower interfacial capacitance formation under no applied external condition (d) higher interfacial capacitance formed under lower applied pressures, which saturates in the higher-pressure regions.

The variation in the pressure sensitivity, both in the high and low regimes, is explained with the help of schematics in figure 7. The high sensitivity in the low-pressure regime might be due to the three primary reasons are the change in the dielectric constant, reduction in the effective distance between the layers of nanofibers, and the change in the effective contact area. Initially, with the application of pressure, the nanofibrous mats are compressed leading to a change in the dielectric constant of S-PVA nanofibers. This is attributed to the presence of air gaps which have relatively lower dielectric constant (ε_r=1) compared to both pure silk (ε_r=2.65) and PVA (ε_r=1.6). The calculated dielectric constant of the S-PVA composite nanofiber was obtained as the 1.71, as shown in the supporting information. The change in dielectric constant results in incremental change in the capacitance due to the directly proportional relationship as described in eq. (2). Figure 7a and 7b demonstrate the change in the inter distance nanometres spacing (d_1, d_2, d_3…. d_n) between the thick multi-layered nanofibers under no pressure and low-pressure conditions.

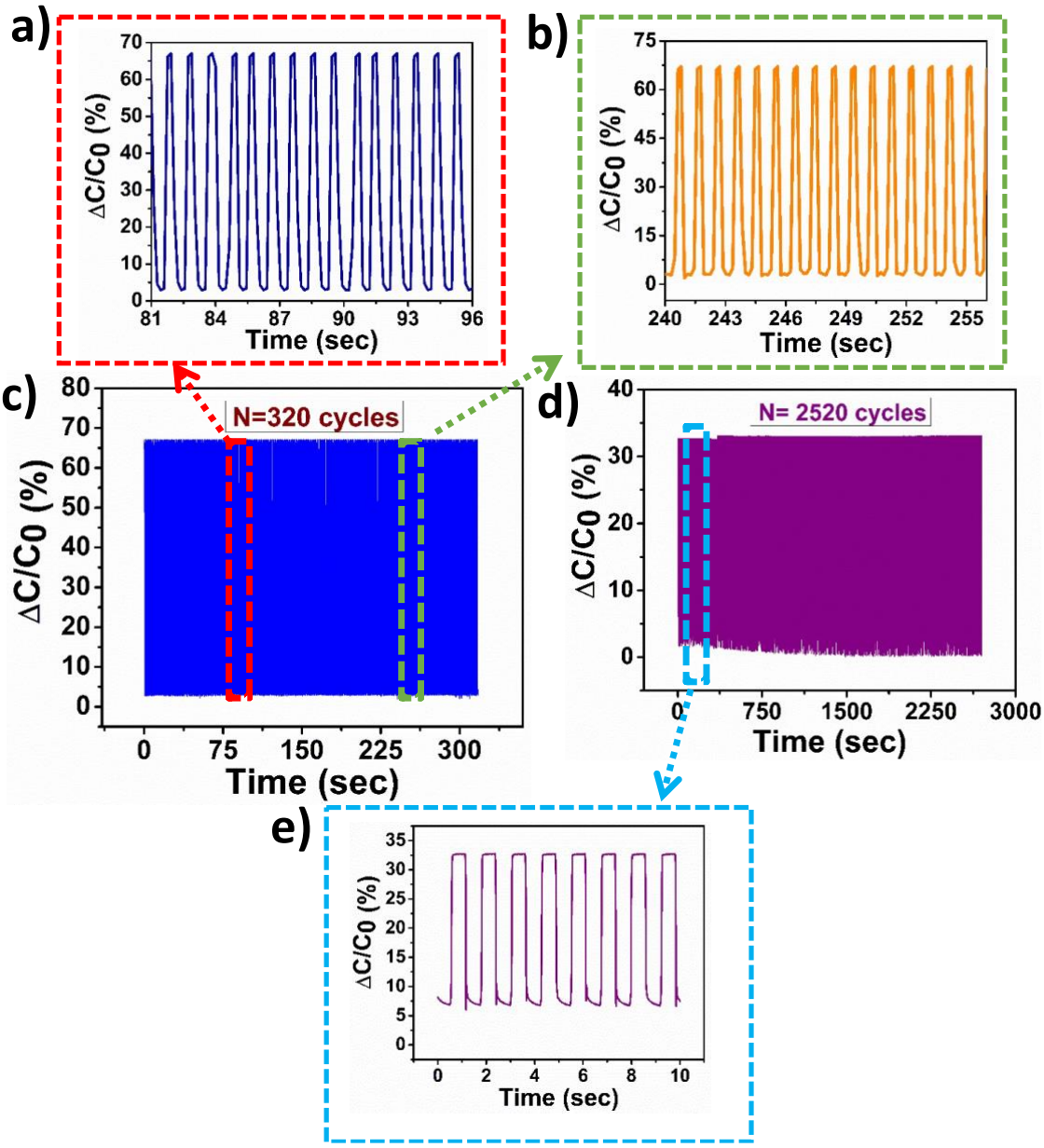

Figure 8. Cyclic repeatability tests under (a), (b) and (c) magnified graph at lower and higher cycles and normal response characteristics of the device respectively under high pressure (400 kPa) for 320 cycles. The magnified images at two different time intervals (start and end position) are also shown, (d) and (e) normal and magnified response plot of the device under low pressure (30 kPa) for 2520 cycles

Due to the applied pressure, there is a decrease in the distance between the nanofibers, resulting in the overall decrease in the effective distance thereby increase in the capacitance in the lower pressure region. In the high-pressure regions, the change in the effective distance is quite low resulting in the lower sensitivity. Further, the contact area between the nanofibers and the electrodes will be minimal without any externally applied pressure due to the highly porous and rough surface as confirmed by the FE-SEM images in figure 4d. In the low power regime (<10kPa),

the electrical double layer (EDL) at the interface of the top and the bottom electrode is very low (figure 7c).

As the applied pressure increases, the contact area between the electrode and the fibre increases and this result in the increase of EDL, thereby exhibiting an incremental change in the interfacial capacitance due to the opposite polarities, as illustrated in figure 7c and 7d. In contrast, in the high-pressure regime, after a certain threshold pressure (100kPa), the change of the effective contact area (and hence the capacitance) is lower, which results in lower sensitivity. To understand the device reliability, cyclic repeatability tests were performed on the S-PVA-based pressure sensor device. Figure 8a, 8b and 8c shows the magnified response plots showing the change in capacitance of the as-fabricated device under high pressure at 400kPa for 320 cycles. The device shows a reliable response, with the inset showing the magnified images at different time intervals at the start and end regions. Similarly, the device was subjected to a moderately low-pressure of less than 30kPa and the response was stable for greater than 2000 cycles, as depicted in figure 8b. Figure 8e shows the magnified image for the duration ranging from (0-10) seconds presenting high repeatability and excellent stability. These results suggest that the as fabricated device is suitable for low-pressure detection applications such as the detection of microphone signals.

To demonstrate the biodegradation, we also fabricated the device with screen-printed silver as the top and bottom electrodes. Figure 9a shows the as prepared flexible and biodegradable chitosan film with an inset showing the screen-printed silver electrode on the chitosan. The change in capacitance with applied pressure is shown in figure 9b. The device exhibits maximum sensitivity of $1.9kPa^{-1}$ in the low-pressure region (<10kPa), $0.184\ kPa^{-1}$ in the medium-pressure region (10-100kPa) and $0.0543\ kPa^{-1}$ in the high-pressure region (100-400kPa). The degradation test was performed by putting the fabricated device in DI water. Figure 9c-9f shows the degradation behaviour of the fabricated S-PVA-based pressure sensor at different times. As soon as the device was placed in the DI water, the chitosan film started to dissolve from both top and bottom. Next, the active layer, S-PVA nanofibers, started to dissolve by absorbing the water due to the excellent hydrophilic nature of PVA.

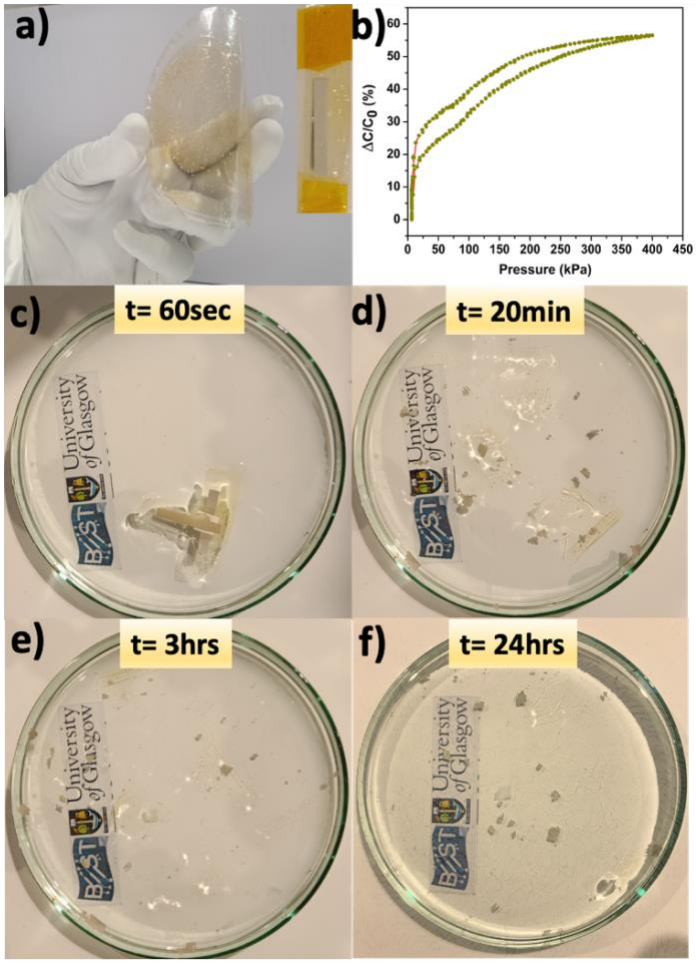

Figure 9. (a) Photograph of chitosan based thin film showing its flexibility. Inset shows screen printed silver electrode (b) relative change in capacitance vs pressure to calculate the sensitivity of silk-PVA based device on chitosan films. Dissolution test of pressure sensor in DI water at different incubation time intervals (c) substrate started to dissolve after 60 seconds (d) physically disintegrated device with silk-PVA nanofibers dissolved completely after 20 minutes (e) 80% of the device dissolved with slight traces of the silver electrodes after 3hours (f) greater than 95% of device dissolved after 24 hours.

It is noteworthy to mention that to achieve a quicker degradability, the chitosan with low molecular weight was chosen to prepare the substrate.[48] The silver electrodes were slowly broken into fine pieces and then wholly got disintegrated from the chitosan substrate, as shown in figure 9d. Here, the screen-printing approach was chosen as it is a cost-effective solution which provide flexibility in terms of large-scale manufacturability. Figure 9e and 9f show the device degradation behaviour after 3 and 24 hours, respectively showing the complete degradation of chitosan and S-PVA with slight traces of disintegrated screen-printed silver electrodes remaining inside the pure DI water. The measured thickness of the chitosan substrate is approximately 500μm. For comparison, similar degradation experiments were performed with different thickness of chitosan films (50, 90, 125 μm thick) prepared by varying spin speeds. As expected, the thinner chitosan films get completely

dissolved in less than 10 hours (approximately), whereas the thicker films dissolved in more than 24 hours. The faster degradation of thinner films matches well with the previous results in the literature.[48] The presented device stands prominent among the other state of the art pressure sensors (Table 1) in terms of both high performance and biodegradability.

Table 1: State of the art comparison based on capacitive pressure sensors.

S.No	Degradability	Active Material	Sensitivity (kPa^{-1}) (max)	$t_{response}$ / $t_{recovery}$ (ms)	Range (kPa)	Cycles (No)	Ref
1	Yes	PLLA	0.7	5/5	0-80	30k	[49]
2	No	PVDF-TrFE-$BaTiO_3$	0.12	150/150	0-400	10k	[50]
3	Yes	PLGA-PCL	0.86	250/170	0-5	5	[9]
4	No	PDMS/ Eco flex	4.1	80/80	0-160	250	[19]
5	Yes	Glycine-Chitosan	0.003V	-	0-10	9k	[10]
6	**Yes**	**Silk-PVA**	**2.8**	**30/40**	**2.5-800**	**2.5k**	**This work**

IV. Conclusion

In our current work, we demonstrated for the first time a fully biocompatible, biodegradable, and mechanically flexible silk-PVA composite nanofiber based capacitive pressure sensor. The sensor was fabricated via a simple, facile, efficient, and cost-effective method. The device demonstrates high sensitivity, wide pressure detection range, quick response, and recovery time of less than 50 milliseconds. The reported high sensitivity of the device was mainly due to the decrease in the effective interlayer distance between the nanofibers and contact area formed at the electrode and highly porous nanofiber interface. Further, the device reveals good cyclic step incremental stability and repeatability under low and high pressures.

III. Experimental Section

A. Materials

Silk cocoons were purchased from the local supplier, UK. Calcium chloride dihydrate ($CaCl_2$ $2H_2O$), Formic acid (FA) (98% pure anhydrous), Polyvinyl alcohol (PVA) of high (Mw) (85000), Sodium carbonate (Na_2CO_3), Chitosan (low molecular weight), Acetic acid, Aluminium foil were procured from the Sigma Aldrich. An ultra-pure deionized (DI) water with resistivity of $18M\Omega cm^{-1}$ was used for all the experiments.

B. Preparation of Silk Solution

The Silk solution was prepared using a methodology similar to the one reported in our previous works.[43] This involves the formic acid-based approach. The step-by-step process for the preparation of the silk fibroin is shown in figure 1. Briefly, the procured silk cocoons were cut into pieces and immersed in the preboiled solution containing 0.05M of Na_2CO_3 in 2000 mL of DI water for 30 minutes to remove the sericin layer coated on the fibroin layer, which is known as the degumming process. Afterwards, the squeeze dried nanofibers were slowly dissolved in the 19:1 ratio of FA to $CaCl_2$ solution under continuous stirring. The prepared silk fibroin solution was casted and dried overnight in a plastic petri dish followed by DI water rinse to completely remove the unwanted $CaCl_2$ which is known to be the regenerated silk fibroin films. Finally, a 10 wt.% silk fibroin solution was prepared by using the Regenerated Silk Fibroin (RSF) in the FA and were further centrifuged to remove any unwanted impurities.

C. Electrospinning of Silk-PVA nanofiber

To obtain the S-PVA solution for electrospinning, an optimized PVA concentration of 2mg/mL was added in the previously prepared 10 wt.% pure transparent and highly viscous silk fibroin solution. A syringe needle of 21G gauge was used with 15 cm distance between the collector and needle and a flow rate of 0.5ml/hr at a high DC voltage of 17 kV. Finally, both the silk and S-PVA nanofibers were collected on a drum collector covered with an aluminium foil.

D. Preparation of Chitosan based thin films

The Chitosan based thin films were prepared by dissolving 1g of chitosan in 4 % (v/v) of acetic acid in DI water at a constant temperature of 50^{o}C, with continuously stirring at 500 rpm. Later, the prepared solution was degassed under vacuum to remove the air bubbles and centrifuged to remove any excess impurities. Finally, the chitosan was casted in a glass petri dish and dried for approximately 48 hours to obtain a flexible and uniform thin film.

E. Material Characterization

The structural characterization was performed using the X-ray diffractogram (XRD) using the Bruker Discover D8 (λ=1.54A^o) and Fourier Transform Infrared Spectroscopy (FTIR) using the Bruker machine with ATR unit attached. XRD measurements were performed on the S-PVA composite nanofibers for a 2θ angles ranging from 10-80^o with a step size of 0.05^o. The FTIR

spectrum of nanofibers was recorded in the transmittance mode with 64 scans for the spectral range varying from the 400-5000 cm^{-1}. The morphological characterization was done using JOEL FE-SEM on both the silk and S-PVA nanofibers.

F. Sensor fabrication and characterization

The vertically stacked capacitive pressure sensors were prepared with S-PVA nanofibers as the dielectric layer and gold on titanium (Ti(10nm)/Au(100nm)) as the top and bottom electrodes using e-beam evaporation. The electrodes of length 2cm and width 0.5 cm were deposited via electron beam evaporation utilizing a hard shadow mask which was made using the computer-controlled blade cutter (Silhoutte Cameo) on a commercial 175µm thick and flexible PVC substrate. The detailed schematic showing complete fabrication steps is included in the supporting information figure 2. The fully biodegradable pressure sensor (substrate and dielectric) was also prepared using the screen-printed silver (2cm x 0.5cm) on a chitosan based thin films as the top and bottom electrode. Uniform device dimensions were maintained for both devices with an active area of ~0.25 cm^2. The sensitivity measurements were performed using an LCR meter (E4980AL Keysight Technologies, USA) with a custom-made LabVIEW 2018 Robotics v18.0f2 (National Instruments, USA). The operating frequency was kept constant at 1MHz throughout experiments to finely capture the minor variations in the capacitance.

Future work:

As a next step towards this work, the fabrication of the different touch sensors using novel 1D and 2D structured materials for multiple sensing such as static and dynamic. The fabrication of capacitive structure based memristor device and the integration of both sensors with memristors and explore towards the e-skin application. Further, we plan to explore memory effect inside the different capacitive sensors due to the structural resemblance with flexible memristors.

References

(1) Nandy, S.; Goswami, S.; Marques, A.; Gaspar, D.; Grey, P.; Cunha, I.; Nunes, D.; Pimentel, A.; Igreja, R.; Barquinha, P.; Pereira, L.; Fortunato, E.; Martins, R. Cellulose: A Contribution for the Zero e-Waste Challenge. *Adv. Mater. Technol.* **2021**, *6* (7), 1–59. https://doi.org/10.1002/admt.202000994.

(2) O. Ozioko, R. Dahiya, Smart Tactile Gloves for Haptic Interaction, Communication, and Rehabilitation, *Advanced Intelligent Systems*, 2100091, 2021..

(3) Pandit, J. A.; Lores, E.; Batlle, D. Cuffless Blood Pressure Monitoring Promises and Challenges. *Clin. J. Am. Soc. Nephrol.* **2020**, *15* (10), 1531–1538. https://doi.org/10.2215/CJN.03680320.

(4) Dahiya, R.; Akinwande, D.; Chang, J. S. Flexible Electronic Skin: From Humanoids to Humans. *Proc. IEEE* **2019**, *107* (10), 2011–2015. https://doi.org/10.1109/JPROC.2019.2941665.

(5) Gao, Y.; Yu, L.; Yeo, J. C.; Lim, C. T. Flexible Hybrid Sensors for Health Monitoring: Materials and Mechanisms to Render Wearability. *Adv. Mater.* **2020**, *32* (15). https://doi.org/10.1002/adma.201902133.

(6) Honjol, Y.; Rajkumar, V. S.; Parent-Harvey, C.; Selvasandran, K.; Kordlouie, S.; Comeau-Gauthier, M.; Harvey, E.; Merle, G. Current View and Prospect: Implantable Pressure Sensors for Health and Surgical Care. *Med. Devices Sensors* **2020**, *3* (3), 1–18. https://doi.org/10.1002/mds3.10068.

(7) Boutry, C. M.; Kaizawa, Y.; Schroeder, B. C.; Chortos, A.; Legrand, A.; Wang, Z.; Chang, J.; Fox, P.; Bao, Z. A Stretchable and Biodegradable Strain and Pressure Sensor for Orthopaedic Application. *Nat. Electron.* **2018**, *1* (5), 314–321. https://doi.org/10.1038/s41928-018-0071-7.

(8) Park, Y.; Kwon, K.; Kwak, S. S.; Yang, D. S.; Kwak, J. W.; Luan, H.; Chung, T. S.; Chun, K. S.; Kim, J. U.; Jang, H.; Ryu, H.; Jeong, H.; Won, S. M.; Kang, Y. J.; Zhang, M.; Pontes, D.; Kampmeier, B. R.; Seo, S. H.; Zhao, J.; Jung, I.; Huang, Y.; Xu, S.; Rogers, J. A. Wireless, Skin-Interfaced Sensors for Compression Therapy. *Sci. Adv.* **2020**, *6* (49), 1–10. https://doi.org/10.1126/sciadv.abe1655.

(9) Khalid, M. A. U.; Ali, M.; Soomro, A. M.; Kim, S. W.; Kim, H. B.; Lee, B. G.; Choi, K. H. A Highly Sensitive Biodegradable Pressure Sensor Based on Nanofibrous Dielectric. *Sensors Actuators, A Phys.* **2019**, *294*, 140–147. https://doi.org/10.1016/j.sna.2019.05.021.

(10) F. Nikbakhtnasrabadi, E. S. Hosseini, S. Dervin, D. Shakthivel, R. Dahiya, Inductor-

Capacitor Resonant Tank based Printed Wireless Pressure Sensor for Online Health Monitoring, *Advanced Electronic Materials*, **2022**. DOI: 10.1002/aelm.202101348.

(11) Ozioko, O.; Karipoth, P.; Escobedo, P.; Ntagios, M.; Pullanchiyodan, A.; Dahiya, R. SensAct: The Soft and Squishy Tactile Sensor with Integrated Flexible Actuator. *Adv. Intell. Syst.* **2021**, *3* (3), 1900145. https://doi.org/10.1002/aisy.201900145.

(12) Karipoth, P.; Pullanchiyodan, A.; Christou, A.; Dahiya, R. Graphite-Based Bioinspired Piezoresistive Soft Strain Sensors with Performance Optimized for Low Strain Values. *ACS Appl. Mater. Interfaces* **2021**. https://doi.org/10.1021/acsami.1c14228.

(13) Park, S. J.; Kim, J.; Chu, M.; Khine, M. Flexible Piezoresistive Pressure Sensor Using Wrinkled Carbon Nanotube Thin Films for Human Physiological Signals. *Adv. Mater. Technol.* **2018**, *3* (1), 1–7. https://doi.org/10.1002/admt.201700158.

(14) Bhattacharjee, M.; Soni, M.; Escobedo, P.; Dahiya, R. PEDOT:PSS Microchannel-Based Highly Sensitive Stretchable Strain Sensor. *Adv. Electron. Mater.* **2020**, *6* (8). https://doi.org/10.1002/aelm.202000445.

(15) Escobedo, P.; Bhattacharjee, M.; Nikbakhtnasrabadi, F.; Dahiya, R. Smart Bandage with Wireless Strain and Temperature Sensors and Batteryless NFC Tag. *IEEE Internet Things J.* **2021**, *8* (6), 5093–5100. https://doi.org/10.1109/JIOT.2020.3048282.

(16) Yogeswaran, N.; Hosseini, E. S.; Dahiya, R. Graphene Based Low Voltage Field Effect Transistor Coupled with Biodegradable Piezoelectric Material Based Dynamic Pressure Sensor. *ACS Appl. Mater. Interfaces* **2020**, *12* (48), 54035–54040. https://doi.org/10.1021/acsami.0c13637.

(17) M. Ntagios, H. Nassar, A. Pullanchiyodan, W. T. Navaraj, R. Dahiya, Robotic Hands with Intrinsic Tactile Sensing via 3D Printed Soft Pressure Sensors, *Advanced Intelligent Systems*, Vol 2, 1900080, **2020**.

(18) Ozioko, O.; Navaraj, W.; Hersh, M.; Dahiya, R. Tacsac: A Wearable Haptic Device with Capacitive Touch-Sensing Capability for Tactile Display. *Sensors (Switzerland)* **2020**, *20* (17), 1–15. https://doi.org/10.3390/s20174780.

(19) Y. Kumaresan, S. Ma, O. Ozioko, R. Dahiya, Soft Capacitive Pressure Sensor with

Enhanced Sensitivity assisted by ZnO NW Interlayers and Airgap, *IEEE Sensors Journal*, **2022**. (DOI: 10.1109/JSEN.2022.3143030)

(20) Lozano Montero, K.; Laurila, M. M.; Peltokangas, M.; Haapala, M.; Verho, J.; Oksala, N.; Vehkaoja, A.; Mäntysalo, M. Self-Powered, Ultrathin, and Transparent Printed Pressure Sensor for Biosignal Monitoring. *ACS Appl. Electron. Mater.* **2021**, *3* (10), 4362–4375. https://doi.org/10.1021/acsaelm.1c00540.

(21) Lee, S.; Reuveny, A.; Reeder, J.; Lee, S.; Jin, H.; Liu, Q.; Yokota, T.; Sekitani, T.; Isoyama, T.; Abe, Y.; Suo, Z.; Someya, T. A Transparent Bending-Insensitive Pressure Sensor. *Nat. Nanotechnol.* **2016**, *11* (5), 472–478. https://doi.org/10.1038/nnano.2015.324.

(22) Nikbakhtnasrabadi, F.; El Matbouly, H.; Ntagios, M.; Dahiya, R. Textile-Based Stretchable Microstrip Antenna with Intrinsic Strain Sensing. *ACS Appl. Electron. Mater.* **2021**, *3* (5), 2233–2246. https://doi.org/10.1021/acsaelm.1c00179.

(23) Guo, J.; Gu, D.; Zhao, T.; Zhao, Z.; Xiong, Y.; Sun, M.; Xin, C.; Zhang, Y.; Pei, L.; Sun, J. Trends in Piezo Channel Research Over the Past Decade: A Bibliometric Analysis. *Front. Pharmacol.* **2021**, *12* (April), 1–14. https://doi.org/10.3389/fphar.2021.668714.

(24) Hosseini, E. S.; Dervin, S.; Ganguly, P.; Dahiya, R. Biodegradable Materials for Sustainable Health Monitoring Devices. *ACS Appl. Bio Mater.* **2021**, *4* (1), 163–194. https://doi.org/10.1021/acsabm.0c01139.

(25) Schmitthenner, H. F.; Barrett, T. M.; Beach, S. A.; Heese, L. E.; Weidman, C.; Dobson, D. E.; Mahoney, E. R.; Schug, N. C.; Jones, K. G.; Durmaz, C.; Otasowie, O.; Aronow, S.; Lee, Y. P.; Ophardt, H. D.; Becker, A. E.; Hornak, J. P.; Evans, I. M.; Ferran, M. C. Modular Synthesis of Peptide-Based Single- And Multimodal Targeted Molecular Imaging Agents. *ACS Appl. Bio Mater.* **2021**, *4* (7), 5435–5448. https://doi.org/10.1021/acsabm.1c00157.

(26) Iqbal, S. M. A.; Mahgoub, I.; Du, E.; Leavitt, M. A.; Asghar, W. Advances in Healthcare Wearable Devices. *npj Flex. Electron.* **2021**, *5* (1), 1–14. https://doi.org/10.1038/s41528-021-00107-x.

(27) D. Shakthivel, A. S. Dahiya, Mukherjee, R. Dahiya, Inorganic Semiconducting Nanowires for Green Energy Solutions, *Current Opinion in Chemical Engineering*, Vol 34, 100753,

2021.

(28) Sasaoka, H. Detection Technologies of Sleep Condition on Bio-Signal Monitoring System. *Proc. SICE Annu. Conf.* **2004**, 825–829.

(29) Jung, M.; Vishwanath, S. K.; Kim, J.; Ko, D. K.; Park, M. J.; Lim, S. C.; Jeon, S. Transparent and Flexible Mayan-Pyramid-Based Pressure Sensor Using Facile-Transferred Indium Tin Oxide for Bimodal Sensor Applications. *Sci. Rep.* **2019**, *9* (1), 1–11. https://doi.org/10.1038/s41598-019-50247-4.

(30) Li, G.; Chen, D.; Li, C.; Liu, W.; Liu, H. Engineered Microstructure Derived Hierarchical Deformation of Flexible Pressure Sensor Induces a Supersensitive Piezoresistive Property in Broad Pressure Range. *Adv. Sci.* **2020**, *7* (18), 1–10. https://doi.org/10.1002/advs.202000154.

(31) Su, Q.; Zou, Q.; Li, Y.; Chen, Y.; Teng, S. Y.; Kelleher, J. T.; Nith, R.; Cheng, P.; Li, N.; Liu, W.; Dai, S.; Liu, Y.; Mazursky, A.; Xu, J.; Jin, L.; Lopes, P.; Wang, S. A Stretchable and Strain-Unperturbed Pressure Sensor for Motion Interference-Free Tactile Monitoring on Skins. *Sci. Adv.* **2021**, *7* (48). https://doi.org/10.1126/sciadv.abi4563.

(32) Hou, C.; Xu, Z.; Qiu, W.; Wu, R.; Wang, Y.; Xu, Q.; Liu, X. Y.; Guo, W. A Biodegradable and Stretchable Protein-Based Sensor as Artificial Electronic Skin for Human Motion Detection. *Small* **2019**, *15* (11), 1–8. https://doi.org/10.1002/smll.201805084.

(33) Xue, J.; Wu, T.; Dai, Y.; Xia, Y. Electrospinning and Electrospun Nanofibers: Methods, Materials, and Applications. *Chem. Rev.* **2019**, *119* (8), 5298–5415. https://doi.org/10.1021/acs.chemrev.8b00593.

(34) Min, G.; Pullanchiyodan, A.; Dahiya, A. S.; Hosseini, E. S.; Xu, Y.; Mulvihill, D. M.; Dahiya, R. Ferroelectric-Assisted High-Performance Triboelectric Nanogenerators Based on Electrospun P(VDF-TrFE) Composite Nanofibers with Barium Titanate Nanofillers. *Nano Energy* **2021**, *90*. https://doi.org/10.1016/j.nanoen.2021.106600.

(35) Kafi, M. A.; Paul, A.; Vilouras, A.; Hosseini, E. S.; Dahiya, R. S. Chitosan-Graphene Oxide-Based Ultra-Thin and Flexible Sensor for Diabetic Wound Monitoring. *IEEE Sens. J.* **2020**, *20* (13), 6794–6801. https://doi.org/10.1109/JSEN.2019.2928807.

(36) Kafi, M. A.; Paul, A.; Vilouras, A.; Dahiya, R. Mesoporous Chitosan Based Conformable and Resorbable Biostrip for Dopamine Detection. *Biosens. Bioelectron.* **2020**, *147* (October 2019), 111781. https://doi.org/10.1016/j.bios.2019.111781.

(37) Bhattacharjee, M.; Vilouras, A.; Dahiya, R. S. Microdroplet-Based Organic Vapour Sensor on a Disposable GO-Chitosan Flexible Substrate. *IEEE Sens. J.* **2020**, *20* (14), 7494–7502. https://doi.org/10.1109/JSEN.2020.2992087.

(38) Dervin, S.; Ganguly, P.; Dahiya, R. S. Disposable Electrochemical Sensor Using Graphene Oxide-Chitosan Modified Carbon-Based Electrodes for the Detection of Tyrosine. *IEEE Sens. J.* **2021**, *21* (23), 26226–26233. https://doi.org/10.1109/JSEN.2021.3073287.

(39) Lee, C.; Kim, S.; Cho, Y. H. Silk and Paper: Progress and Prospects in Green Photonics and Electronics. *Adv. Sustain. Syst.* **2020**. https://doi.org/10.1002/adsu.202000216.

(40) Yong, J.; Hassan, B.; Liang, Y.; Ganesan, K.; Rajasekharan, R.; Evans, R.; Egan, G.; Kavehei, O.; Li, J.; Chana, G.; Nasr, B.; Skafidas, E. A Silk Fibroin Bio-Transient Solution Processable Memristor. *Sci. Rep.* **2017**, *7* (1), 1–12. https://doi.org/10.1038/s41598-017-15395-5.

(41) Thanyacharoen, T.; Chuysinuan, P.; Techasakul, S.; Nooeaid, P.; Ummartyotin, S. Development of a Gallic Acid-Loaded Chitosan and Polyvinyl Alcohol Hydrogel Composite: Release Characteristics and Antioxidant Activity. *Int. J. Biol. Macromol.* **2018**, *107* (PartA), 363–370. https://doi.org/10.1016/j.ijbiomac.2017.09.002.

(42) He, F.; You, X.; Gong, H.; Yang, Y.; Bai, T.; Wang, W.; Guo, W.; Liu, X.; Ye, M. Stretchable, Biocompatible, and Multifunctional Silk Fibroin-Based Hydrogels toward Wearable Strain/Pressure Sensors and Triboelectric Nanogenerators. *ACS Appl. Mater. Interfaces* **2020**, *12* (5), 6442–6450. https://doi.org/10.1021/acsami.9b19721.

(43) Gunapu, D. V. S. K.; Prasad, Y. B.; Mudigunda, V. S.; Yasam, P.; Rengan, A. K.; Korla, R.; Vanjari, S. R. K. Development of Robust, Ultra-Smooth, Flexible and Transparent Regenerated Silk Composite Films for Bio-Integrated Electronic Device Applications. *Int. J. Biol. Macromol.* **2021**, *176*, 498–509. https://doi.org/10.1016/j.ijbiomac.2021.02.051.

(44) Kundu, J.; Chung, Y. Il; Kim, Y. H.; Tae, G.; Kundu, S. C. Silk Fibroin Nanoparticles for

Cellular Uptake and Control Release. *Int. J. Pharm.* **2010**, *388* (1–2), 242–250. https://doi.org/10.1016/j.ijpharm.2009.12.052.

(45) Dodel, M.; Nejad, N. H.; Bahrami, S. H.; Soleimani, M.; Hanaee-Ahvaz, H. Modifying the Mechanical Properties of Silk Nanofiber Scaffold by Knitted Orientation for Regenerative Medicine Applications. *Cell. Mol. Biol.* **2016**, *62* (10), 16–25. https://doi.org/10.14715/cmb/2016.62.10.3.

(46) Lee, S. J.; Atala, A.; Zhang, J.; Wehrle, E.; Wang, L.; Nan, X.; Alloy, I. Development of Novel Silk Fibroin / Polyvinyl Alcohol / Sol – Gel Bioactive Glass Composite Matrix by Modified Layer by Layer Electrospinning Method for Bone Tissue Construct Generation Development of Novel Silk Fi Broin / Polyvinyl Alcohol / Sol – Gel Bi.

(47) Lin, M. F.; Xiong, J.; Wang, J.; Parida, K.; Lee, P. S. Core-Shell Nanofiber Mats for Tactile Pressure Sensor and Nanogenerator Applications. *Nano Energy* **2018**, *44* (November 2017), 248–255. https://doi.org/10.1016/j.nanoen.2017.12.004.

(48) Usman, A.; Zia, K. M.; Zuber, M.; Tabasum, S.; Rehman, S.; Zia, F. Chitin and Chitosan Based Polyurethanes: A Review of Recent Advances and Prospective Biomedical Applications. *Int. J. Biol. Macromol.* **2016**, *86*, 630–645. https://doi.org/10.1016/j.ijbiomac.2016.02.004.

(49) Boutry, C. M.; Kaizawa, Y.; Schroeder, B. C.; Chortos, A.; Legrand, A.; Wang, Z.; Chang, J.; Fox, P.; Bao, Z. Pressure Sensor for Orthopaedic Application. *Nat. Electron.* **2018**, *1* (May).

(50) Ma, L.; Yu, X.; Yang, Y.; Hu, Y.; Zhang, X.; Li, H.; Ouyang, X.; Zhu, P.; Sun, R.; Wong, C. ping. Highly Sensitive Flexible Capacitive Pressure Sensor with a Broad Linear Response Range and Finite Element Analysis of Micro-Array Electrode. *J. Mater.* **2020**, *6* (2), 321–329. https://doi.org/10.1016/j.jmat.2019.12.008.